Nonadiabatic decay of Rydberg-atom–ion molecules

A. Duspayev* and G. Raithel
Department of Physics, University of Michigan, Ann Arbor, Michigan 48109, USA

(Received 1 September 2021; accepted 20 December 2021; published 14 January 2022)

The decay of Rydberg-atom–ion molecules (RAIMs) due to nonadiabatic couplings between electronic potential-energy surfaces is investigated. We employ the Born-Huang representation and perform numerical simulations using a Crank-Nicolson algorithm. The nonadiabatic lifetimes of rubidium RAIMs for the lowest ten vibrational states, ν, are computed for selected Rydberg principal quantum numbers, n. The nonadiabatic lifetimes are found to generally exceed the radiative Rydberg-atom lifetimes. We observe and explain a trend of the lifetimes as a function of ν and n, and attribute irregularities to quantum interference arising from a shallow potential well in an inner potential surface. Our results will be useful for future spectroscopic studies of RAIMs.

DOI: 10.1103/PhysRevA.105.012810

I. INTRODUCTION

Ultralong-range Rydberg molecules (ULRM) [1,2] are an active direction in Rydberg-atom research. ULRMs can be distinguished based upon their formation mechanisms. For instance, in Rydberg-ground molecules [3,4] a ground-state atom resides within the Rydberg-atom wave function, and a molecular bond is formed due to scattering of the Rydberg electron at the perturber atom. The studies on this type of ULRMs include detailed analyses of association [5–11], electronic structure [12], spin-orbit coupling [13–15] and scattering processes [16–19], calculations and measurements of lifetimes [20–22] and permanent electric dipole moments [23] that can vary from a few [24,25] to thousands of debyes [26,27], and interactions with external fields [28–30]. In another type of Rydberg molecules, referred to as macrodimers [31–33], two [31] or more [34] Rydberg atoms with nonoverlapping wave functions (LeRoy radius condition [35]) become bounded via multipolar interactions [36–39]. Their formation [40–43], vibrational structure [44], lifetimes [32,33,45], and alignment with external fields [46] have been studied.

Recently, a Rydberg-atom–ion molecule (RAIM) [47,48] has been proposed that opens new perspectives at the interface between the fields of Rydberg molecules and atom-ion interactions [49–56]. In RAIMs, multipolar interaction between a Rydberg atom and an ion outside of the atom leads to bound molecular states. The nonadiabatic decay rate of RAIMs was predicted to be negligibly small [47,48], based upon Landau-Zener (LZ) tunneling probabilities. Since the assumptions of LZ tunneling are not satisfied in RAIMs, as discussed in Sec. IV, a quantum theory is needed to obtain accurate values for the nonadiabatic lifetimes of RAIMs.

Here, we study the nonadiabatic dynamics of RAIMs utilizing the Born-Huang representation (BHR) [57], in which the vibrational motion is treated fully quantum mechanically and nonadiabatic couplings are accurately described. Being a common method to study nonadiabatic processes in conventional molecules [58], the BHR has also been used previously in studies on Rydberg-ground [59,60] and Rydberg-Rydberg molecules [44]. Here we utilize it to calculate decay times of RAIMs due to nonadiabatic transitions. After reviewing the basic theory of RAIMs in Sec. II, we discuss the BHR in Sec. III. Results for selected RAIMs are presented and discussed in Sec. IV. The paper is concluded in Sec. V.

II. THEORY OF RYDBERG-ATOM–ION MOLECULES

The theory of RAIMs has been developed in [47]. RAIMs, sketched in Fig. 1(a), are formed between an ion and a neutral Rydberg atom via electric-multipole interaction. The internuclear distance R is larger than the radius of the Rydberg atom. Adopting a z axis aligned with the internuclear axis and assuming a pointlike positive ion, the interaction is, in atomic units [37,38,42],

$$V_{\mathrm{int},m_J}(\hat{\mathbf{r}}_e;R) = -\sum_{l=1}^{l_{\max}} \sqrt{\frac{4\pi}{2l+1}}\frac{\hat{r}_e^{\,l}}{R^{l+1}} Y_{l0}(\hat{\theta}_e,\hat{\phi}_e). \qquad (1)$$

Here, m_J is the conserved magnetic quantum number of the Rydberg atom, n the principal quantum number, ℓ the orbital quantum number, $\hat{\mathbf{r}}_e = (\hat{r}_e, \hat{\theta}_e, \hat{\phi}_e)$ the Rydberg-electron position operator relative to the atom's center, and $Y_{l0}(\hat{\theta}_e, \hat{\phi}_e)$ a spherical harmonic in which l is the multipole order of the atomic charge distribution. Diagonalization of the Hamiltonian with atom-ion interaction given in Eq. (1) yields the molecular potential-energy curves (PECs). Some PECs exhibit deep wells conducive to bound vibrational states of RAIMs, such as PECs in the vicinity of nP_J Rydberg states of cesium and rubidium. The characteristics of these RAIMs depend on quantum defects and other atomic parameters [47,48].

In Fig. 1(b), we show a case in which RAIMs are formed below the Rb $45P$ asymptotes. The RAIM potential wells are several hundreds of MHz deep and on the order of 100 nm wide, which leads to tens of bound vibrational states. In Fig. 1(c), we show the lowest five RAIM states in the

*alisherd@umich.edu

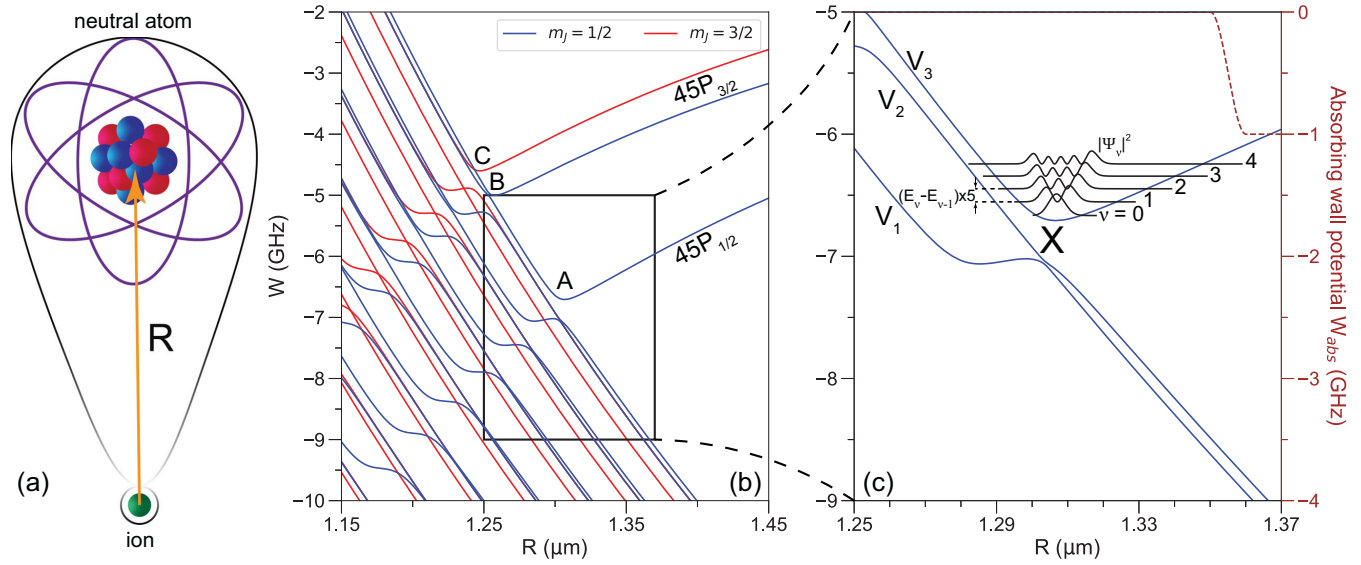

FIG. 1. (a) Sketch of the RAIM. (b) Potential-energy curves (PECs) of rubidium RAIMs for $m_J = 1/2$ and $3/2$ as a function of internuclear distance R. Energies are relative to the field-free atomic $45P_{3/2}$ state. The wells in the regions A, B, and C are expected to support RAIMs. (c) Magnified view of the region A with the three $m_J = 1/2$ PECs used in our calculation of nonadiabatic decay, and wave-function densities of the five lowest RAIM vibrational states in the PEC labeled V_3. The vertical offsets between the baselines of the wave-function densities correspond to energy intervals between the corresponding vibrational states multiplied by a factor of 5. The "X" marks the most relevant anticrossing. The imaginary absorbing-wall potential $W_{\rm abs}$ used in the computational approach is also shown.

molecular PEC labeled V_3. The stability of the vibrational states may be affected by the nonadiabatic couplings between V_3 and neighboring PECs, labeled V_1 and V_2 in Fig. 1(c). The wave-function densities of the lowest vibrational states on V_3 extend over distances on the order of or less than the width of the anticrossing marked "X." The analysis of nonadiabatic decay therefore requires a quantum-mechanical treatment of both the electronic and the vibrational dynamics.

III. NONADIABATIC DYNAMICS

A. Time-dependent Schrödinger equation

In the Born-Oppenheimer approximation (BOA) [61], electronic and nuclear wave functions are adiabatically separated to facilitate the calculation of vibrational molecular states. However, the BOA can "break down" when vibrational and electronic time scales approach each other, as is the case when PECs exhibit narrow anticrossings, leading to nonadiabatic coupling of PECs and to molecular decay. In Fig. 1(c), nonadiabatic coupling from V_3 to the unbound PECs may contribute significantly to RAIM decay.

Writing the time-dependent Schrödinger equation (TDSE) in BHR [57] (see [58] and references therein for a recent overview of BHR theory and applications) allows us to incorporate nonadiabatic effects. To that end, we consider the vibrational degree of freedom of a diatomic RAIM along its internuclear axis, $\hat{\mathbf{R}}$. The TDSE in BHR is written as

$$i\hbar\frac{\partial\psi_i(R,t)}{\partial t} = -\frac{\hbar^2}{2\mu}\frac{\partial^2\psi_i(R,t)}{\partial R^2} + V_i(R)\psi_i(R,t) + \sum_j \mathcal{F}_{ij}(R)\psi_j(R,t). \quad (2)$$

Here, $\psi_i(R,t)$ is the adiabatic vibrational RAIM wave function on $V_i(R)$, μ is the reduced mass, and the $\mathcal{F}_{ij}(R)$ are the nonadiabatic couplings between the adiabatic wave functions on PECs V_i and on V_j. The nonadiabatic terms of the BHR, $\mathcal{F}_{ij}(R)$, couple nuclear and electronic motion. Explicitly,

$$\mathcal{F}_{ij}(R) = \mathcal{A}_{ij}(R)\frac{\partial}{\partial R} + \mathcal{B}_{ij}(R), \quad (3)$$

where $\mathcal{A}_{ij}(R)$ is referred to as the first-order nonadiabatic coupling and is defined as (in one dimension)

$$\mathcal{A}_{ij}(R) = -\frac{\hbar^2}{\mu}\langle\phi_i|\frac{\partial}{\partial R}|\phi_j\rangle. \quad (4)$$

Here, $|\phi_i(R)\rangle$ are the R-dependent electronic states of the Rydberg atom, with wave functions $\phi_i(\mathbf{r}_e;R) = \langle\mathbf{r}_e|\phi_i(R)\rangle$. The inner product in Eq. (4) is evaluated in the Rydberg-electron state space; i.e., it involves, in principle, an integral over $\mathbf{r}_e$. In practice, the Rydberg state is represented in the "diabatic" Rydberg-state basis $\{|n,\ell,J,m_J\rangle =: |\alpha\rangle\}$, with the shorthand α for all diabatic-state quantum numbers. The electronic wave function on PEC i then reads

$$\phi_i(\mathbf{r}_e;R) = \sum_\alpha c_{i,\alpha}(R)\langle\mathbf{r}_e|\alpha\rangle,$$

with coefficient functions $c_{i,\alpha}(R)$. Because of the R independence and the orthonormality of the $|\alpha\rangle$,

$$\mathcal{A}_{ij}(R) = -\frac{\hbar^2}{\mu}\sum_\alpha c^*_{i,\alpha}(R)\left[\frac{\partial}{\partial R}c_{j,\alpha}(R)\right]. \quad (5)$$

The $\mathcal{B}_{ij}(R)$ in Eq. (3) is referred to as the second-order nonadiabatic coupling and is

$$\mathcal{B}_{ij}(R) = -\frac{\hbar^2}{2\mu}\langle\phi_i|\frac{\partial^2}{\partial R^2}|\phi_j\rangle = -\frac{\hbar^2}{2\mu}\sum_{\alpha} c^*_{i,\alpha}(R)\left[\frac{\partial^2}{\partial R^2}c_{j,\alpha}(R)\right]. \quad (6)$$

Since $\mathcal{A}_{ij}(R) = -\mathcal{A}_{ji}(R)$, it is $\mathcal{A}_{ii}(R) = 0$. The generally nonzero diagonal second-order nonadiabatic couplings, $\mathcal{B}_{ii}(R)$, are often combined with the corresponding $V_i(R)$ into

$$\tilde{V}_i(R) = V_i(R) + \mathcal{B}_{ii}(R). \quad (7)$$

We may then rewrite Eqs. (2) and (3) as

$$i\hbar\frac{\partial\psi_i(R,t)}{\partial t} = -\frac{\hbar^2}{2\mu}\frac{\partial^2\psi_i(R,t)}{\partial R^2} + \tilde{V}_i(R)\psi_i(R,t) + \sum_{j\neq i}\left[\mathcal{A}_{ij}(R)\frac{\partial\psi_j(R,t)}{\partial R} + \mathcal{B}_{ij}(R)\psi_j(R,t)\right]. \quad (8)$$

We refer to $\tilde{V}_i(R)$ as "adiabatic potentials," i.e., potentials in which all diagonal nonadiabatic energy shifts of the adiabatic states have been added to the PECs, $V_i(R)$. We also note that for $\mathcal{B}$ we have

$$\mathcal{B}_{ij} + \mathcal{B}^*_{ji} = -\frac{\hbar^2}{\mu}\left[\frac{\partial}{\partial R}\langle\phi_i|\right]\left[\frac{\partial}{\partial R}|\phi_j\rangle\right].$$

We use this identity as a check for numerical errors caused by the step size in R.

It is apparent from Eqs. (4)–(6) that the nonadiabatic couplings follow from the R dependencies of the adiabatic Rydberg states $|\phi_i(R)\rangle$, which are critically affected by the avoided crossings between the PECs. As the general shapes of the PECs are the same for all cases studied here, in Sec. IV we find a general trend for the nonadiabatic RAIM decay times. However, detailed differences in the nonadiabatic $\mathcal{A}$ and $\mathcal{B}$ terms and in the wave-function dynamics on the dissociative PECs lead to peculiar quantum effects that are also discussed.

B. Simulation method

We first numerically calculate PECs for selected Rydberg states nP_J of ^{87}Rb [see, for instance, Fig. 1(b) for $45P_J$]. We investigate bound RAIM vibrational states on PECs that asymptotically connect with the $nP_{1/2}$ levels. The corresponding PEC for $n = 45$ is labeled V_3 in Fig. 1(c). This PEC, and equivalent PECs for other n values, exhibit nonadiabatic couplings mostly to a pair of lower, dissociating PECs labeled V_1 and V_2 in Fig. 1(c). The PEC calculation yields the PECs, the associated adiabatic Rydberg states $|\phi_i(R)\rangle$, and the nonadiabatic terms $\mathcal{A}_{ij}(R)$ and $\mathcal{B}_{ij}(R)$ according to the equations in Sec. III A. In view of the structure of the PEC anticrossings evident in Fig. 1, the effect of nonadiabatic couplings of V_3 to PECs other than V_1 and V_2 is deemed negligible. The Rydberg-state basis sets used in the PEC calculations include all Rydberg levels with $m_J = 1/2$ and effective principal quantum number differing by less than five from that of the molecular RAIM states of interest.

The computational method to solve the TDSE in Eq. (8) on the three relevant PECs V_1, V_2, and V_3 is a Crank-Nicolson (CN) algorithm [62]. The simulation is initialized with a RAIM vibrational state on the adiabatic potential $\tilde{V}_3$ [which differs slightly from the PEC V_3, according to Eq. (7)]. Over the course of the subsequent simulated evolution, the norm of the wave function decays due to the nonadiabatic couplings, allowing us to extract the molecular lifetimes. In the following, we describe additional details of the method.

The potential $\tilde{V}_3(R)$, constructed according to Eq. (7), is used to calculate the initial vibrational RAIM state, $\Psi_\nu(R)$, with vibrational quantum number ν. The initial state for the CN simulation then is $\psi_1(R, t = 0) = \psi_2(R, t = 0) = 0$ and $\psi_3(R, t = 0) = \Psi_\nu(R)$. The wave function is propagated in time for a duration of $t_{\text{total}} = 50\,\mu$s with a step size $\Delta t =$ 20 ps. In order to reduce transients from sudden "turn-on" of the nonadiabatic terms, the nonadiabatic terms $\mathcal{A}_{ij}(R)$ and $\mathcal{B}_{ij}(R)$ are slowly ramped up at the beginning of the time propagation. We still find minor initial transients in the $\psi_i(R, t)$, which cease at times $t_0 \sim 10$ ns.

The dissociating potentials, V_1 and V_2, are unbound. As our CN simulation employs a spatial box with fixed boundary conditions $\psi_i(R) = 0$ on all boundaries, the potentials must be modified such that wave functions propagating outward on V_1 and V_2 are absorbed rather than reflected. To terminate the outgoing wave function, we add an imaginary part, $\text{Im}[V_i] = W_{i,\text{abs}}(R)$, on the unbound potentials V_1 and V_2, as depicted by the dashed line in Fig. 1(c). The domain over which $W_{i,\text{abs}}(R)$ differs from zero is placed far enough out in R that it does not affect the nonadiabatic dynamics of interest, which is restricted to regions within which the nonadiabatic couplings differ from zero. The absorbing wall $W_{i,\text{abs}}(R)$ exhibits a smooth turn-on, so as to avoid reflections. We have checked the effectiveness of the absorbing wall as well as the absence of wall reflections by calculating the quantum flux as a function of R (outside and inside the wall), and by verifying the absence of standing-wave patters on ψ_1 and ψ_2 near the absorbing wall.

The absorbed outgoing flux leads to a decay of the overall wave-function norm [63], allowing us to extract the RAIM lifetime. The population in ψ_3, $p_3(t) = \int |\psi_3(R, t)|^2 dR$, is determined as a function of propagation time and fitted to the function

$$p_3(t) = p_3(t_0)e^{-(t-t_0)/\tau_{\text{nad}}}, \quad (9)$$

with fitting parameters $p_3(t_0)$ and τ_{nad}. Here, $p_3(t_0) \lesssim 1$ reflects the population after ramping up the nonadiabatic terms and after allowing transients to cease, and τ_{nad} is the nonadiabatic RAIM lifetime for the given n and ν.

Although most τ_{nad} values are longer than t_{total}, as seen in Fig. 2, the decrease of $p_3(t)$ during the interval t_{total} allows for an accurate determination of τ_{nad} in all cases studied. We have checked that lowering the computation time step Δt does not significantly alter the τ_{nad}.

IV. RESULTS AND DISCUSSION

We obtain the nonadiabatic lifetimes, τ_{nad}, of the lowest ten vibrational states of RAIMs below the $nP_{1/2}$ Rydberg-state asymptotes for n ranging from 25 to 65 with a step of 5. The

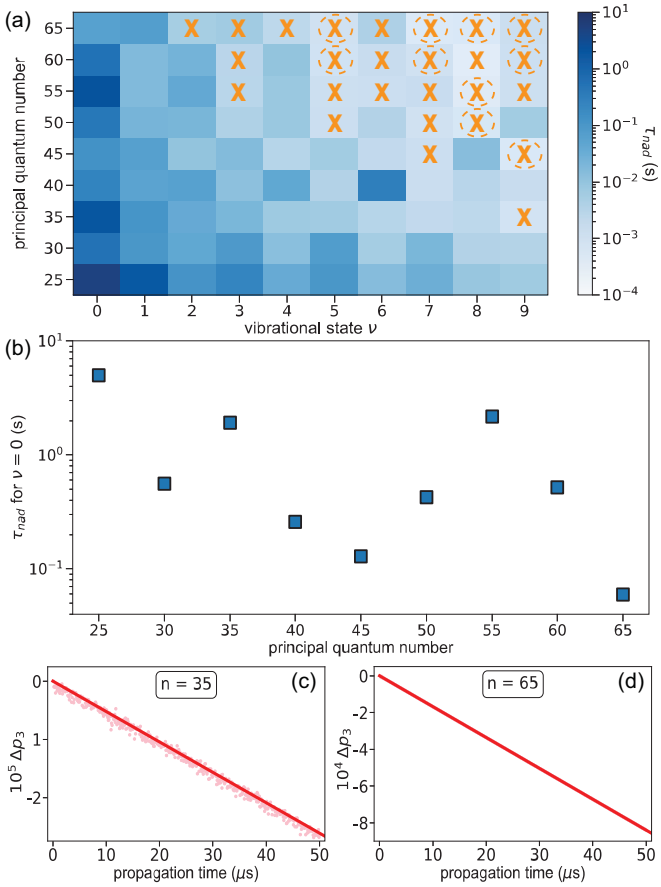

FIG. 2. (a) Calculated nonadiabatic lifetimes, $\tau_{\rm nad}$, of rubidium RAIMs below the $nP_{1/2}$ asymptotes vs vibrational and principal quantum numbers, ν and n, displayed on the indicated logarithmic color scale. The "X" and dashed circles mark cases in which $\tau_{\rm nad}$ is less than ten times the radiative decay time at 1.2 and 300 K, respectively. (b) The lifetimes $\tau_{\rm nad}$ for the ground vibrational state, $\nu = 0$, corresponding to the first column in panel (a). (c) The computed population decrease, $\Delta p_3(t)$, of the ground RAIM states for $n = 35$ as a function of time. (d) Same as panel (c) but for $n = 65$. The $\tau_{\rm nad}$ values follow from the slopes according to Eq. (9).

results are listed in Table I and visualized in Fig. 2(a). These lifetimes are much longer than the radiative lifetimes of nP Rydberg states, τ_r, which have values between $\tau_r = 32\,\mu$s for $n = 25$ and $680\,\mu$s for $n = 65$ in a 1.2-K blackbody radiation field. In 300-K radiation fields, the τ_r values are between 17 and $160\,\mu$s for $n = 25$ and 65, respectively, because upward and downward bound-bound transitions as well as thermal ionization reduce the lifetime [64]. Our τ_r values, obtained in context with work involving Rydberg-atom-state diffusion in thermal radiation fields [65,66], are roughly inline with values of $\approx 20\,\mu$s at $n = 25$ [67] and $\approx 150\,\mu$s at $n = 65$ [68] reported elsewhere.

Under the absence of other decay channels, the net RAIM decay time $\tau = (1/\tau_{\rm nad} + 1/\tau_r)^{-1}$. The symbols on the color map in Fig. 2(a) mark cases in which $\tau_{\rm nad} < 10\tau_r$ in 1.2- and 300-K blackbody fields. Figure 2(a) shows that nonadiabatic RAIM decay, while not being the dominant decay mechanism, should have a noticeable effect at higher n values and vibrational quantum numbers ν. We note that the values for τ_r assumed in Fig. 2(a) are for nP Rydberg states, whereas the electronic states of RAIMs carry up to about 50% admixture of longer-lived high-ℓ Rydberg levels. This means nonadiabatic decay might be slightly more relevant, on a relative scale, than suggested in Fig. 2(a).

The LZ model is inadequate for low-lying vibrational states of RAIMs, mostly due to the following reasons. Foremost, the LZ model is classical in the external degree of freedom, while in the problem at hand the dynamics in the external degree of freedom is in the quantum domain. If one were to adopt a classical description, the Rydberg-molecule motion in the vibrational ground state would scan only a fraction of the anticrossing width, as would be the case in Fig. 1(c), whereas the LZ model requires five or more anticrossing widths for the LZ tunneling probability to approach its asymptotic value to within a few percent [69,70]. Further, the classical scan velocity in the LZ model is assumed to be fixed within the anticrossing region, whereas in the RAIMs studied here the classical vibrational velocity has an approximately sinusoidal time dependence within the anticrossing region.

To give an illustration of the inadequacy of LZ estimates for nonadiabatic RAIM decay, we consider the RAIM vibrational ground state for $45P_J$, for which we have computed $\tau_{\rm nad} \sim 0.13$ s [see Fig. 2(b) and Table I]. From the PECs in Fig. 1 and the vibrational energy levels we estimate a vibration frequency of $f_0 = 18.2$ MHz, corresponding to a LZ decay "attempt rate" of $R_t = 2f_0 = 36.4$ MHz. The main avoided crossing has a gap size of $G \approx h \times 350$ MHz [see gap marked "X" in Fig. 1(c)]. The differential slope of the level crossing, estimated from Fig. 1(b), is $s = h \times 49\,{\rm GHz}/\mu{\rm m}$.

TABLE I. Calculated nonadiabatic lifetimes $\tau_{\rm nad}$ in seconds.

ν	$n = 25$	$n = 30$	$n = 35$	$n = 40$	$n = 45$	$n = 50$	$n = 55$	$n = 60$	$n = 65$
0	4.99	0.560	1.91	0.259	0.129	0.43	2.180	0.52	0.0595
1	1.67	0.105	0.116	0.0547	0.0627	0.0231	0.0175	0.0172	0.0724
2	0.123	0.04513	0.0393	0.0600	0.0105	0.02228	0.0425	0.0245	0.00570
3	0.238	0.0905	0.0216	0.012674	0.0167	0.004007	0.00297	0.002806	0.00659
4	0.0367	0.01292	0.00773	0.0439	0.00324	0.008205	0.00855	0.01074	0.00259
5	0.103	0.0763	0.00685	0.003692	0.00631	0.0013225	0.00122	0.0009615	0.00103
6	0.0151	0.005743	0.00320	0.31	0.00219	0.003768	0.00135	0.001697	0.00426
7	0.0295	0.02190	0.00221	0.0015027	0.00132	0.001016	0.00162	0.0010159	0.000475
8	0.00920	0.003701	0.00262	0.003154	0.0143	0.0006540	0.000411	0.0003662	0.000534
9	0.00702	0.003612	0.000851	0.001656	0.000572	0.00655	0.00120	0.001261	0.00139

For a LZ RAIM decay estimate, in a first try we assume a fixed particle velocity given by the molecule's classical vibration velocity, $v_{\max}$, at the minimum of V_3. From $(\mu/2)v_{\max}^2 = hf_0/2$, with effective mass $\mu = 43.5$ amu for ^{87}Rb, we obtain $v_{\max} = 0.41$ m/s. In terms of the commonly used variable $\Gamma = G^2/(4\hbar s\, v_{\max}) = 9.58$, the LZ tunneling probability then is $P_{\rm LZ} = \exp(-2\pi\Gamma) = 7 \times 10^{-27}$, and the LZ RAIM lifetime $\tau_{\rm LZ} = 1/(R_t P_{\rm LZ}) = 4 \times 10^{18}$ s. This estimate is about 20 orders of magnitude too large. In a second try, the vibrational energy is referenced to the midpoint between the PECs. This leads to $v_{\max} = 1.86$ m/s and $\tau_{\rm LZ} = 0.016$ s, which is about one order of magnitude too small.

The vast amount of variation caused by a $v_{\max}$ change of a factor of 4.5 is due to the exponential dependence of $\tau_{\rm LZ}$ on $2\pi\Gamma$. Similarly, $\tau_{\rm LZ}$ depends strongly on the exact values for the LZ coupling strength, $G/2$, and the differential slope, s. The values of G and s, which are not perfectly well defined in RAIM PECs, are estimated from Fig. 1(c) and carry uncertainties on the order of 10% each, leading to an absolute uncertainty in Γ of about 2, corresponding to about five orders of magnitude in $\tau_{\rm LZ}$. The example discussed here shows that nonadiabatic-lifetime estimates based on the semiclassical LZ model are questionable. Importantly, a quantum calculation is required in order to be able to drop a number of assumptions made in the LZ model that are false for low RAIM vibrational states, such as adopting a classical description of vibrational motion in the quantum domain, assuming a fixed scan velocity through the anticrossing region, assuming a fixed differential slope s, and assuming a fixed coupling strength $G/2$. Quantum interference effects in the external degree of freedom, found to be important in the remainder of this section, are also not covered in the semiclassical LZ tunneling picture.

From Fig. 2 and Table I it is seen that the nonadiabatic lifetimes follow a downward trend with increasing n and increasing ν. This is expected because the anticrossing gaps decrease with increasing n, and because the $\partial/\partial R$ operator, which occurs in combination with the $\mathcal{A}$ terms, exacerbates the nonadiabatic coupling at higher ν values, where the vibrational wave-function gradients become larger.

Inspecting Fig. 2 and Table I, we further note substantial deviations of $\tau_{\rm nad}$ from the overall trend. E.g., the $\tau_{\rm nad}$ values for the $\nu = 0$ states for $n = 35$ and 55 stand out against the overall trend. We believe that the irregularities originate in a quantum-interference effect in the RAIM decay. It has been shown in other contexts that quantum interference can affect the decay dynamics of other molecules [71] and experimental spectroscopic signals [72]. To illustrate quantum interference in RAIM decay, in Fig. 3 we show PECs V_1 and V_3 and their adiabatic wave-function densities. The nonadiabatic couplings set up a quasistationary ψ_1 and an associated probability-density flow that causes the nonadiabatic RAIM decay. The density $|\psi_1|^2$ relative to $|\psi_3|^2$ is small, but nonzero (even at the right margin of the plot), and it exhibits a standing wave in a shallow well in V_1 centered around $\approx$2.20 μm. The standing wave is due to a 100% reflection on the rising side of V_1 near 2.18 μm, and a partial quantum reflection at the three-level crossing near 2.23 μm. The net outward flow on V_1 to the right of the anticrossing is a superposition of a contribution due to direct nonadiabatic coupling from V_3 onto V_1, and a contribution that proceeds via nonadiabatic coupling from V_3 into the shallow potential well in V_1 and time-delayed escape, as visualized by the delay loop in Fig. 3. The superposition amplitude depends on the phase difference between the contributions, which varies as a function of n and ν, causing the irregularities seen in Fig. 2. A few combinations of n and ν appear to exhibit substantial destructive interference, leading to lifetimes that are much longer than the overall trend would suggest.

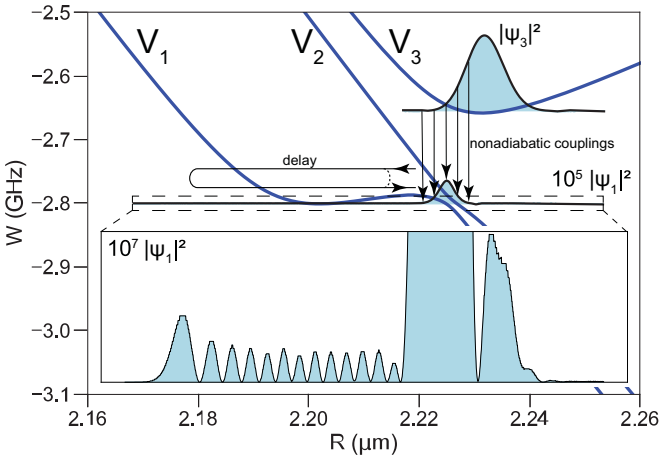

FIG. 3. Wave-function densities $|\psi_1|^2$ and $|\psi_3|^2$ in the respective potentials V_1 and V_3 after reaching a quasisteady state for $55P_{1/2}$. The inset shows an enlarged view of $|\psi_1|^2$.

The situation portrayed in Fig. 3 applies to all values of n studied. Our interpretation of the lifetime irregularities in Fig. 2 in terms of a quantum interference effect has been supported in additional test calculations, not shown, in which an absorbing potential has been placed within the shallow potential well in V_1. The test calculations show a smooth dependence of $\tau_{\rm nad}$ without irregularities. Quantum interference effects in RAIMs could be an interesting topic for future detailed studies.

V. CONCLUSION

In summary, we have presented results of calculations of nonadiabatic decay of Rydberg-atom–ion molecules of Rb. The lifetimes, extracted for nine representative values of n and for the lowest ten vibrational states, follow an overall trend that is inline with the behavior of avoided-crossing gap sizes and the structure of the vibrational wave functions. Deviations from the trend were attributed to a quantum interference effect. Our results confirm that the RAIM states are quite stable against nonadiabatic decay, and that their lifetimes are mainly limited by radiative decay of the Rydberg valence electron. The relevance of nonadiabatic decay could be demonstrated in the future by testing molecular states with principal and vibrational quantum numbers for which the nonadiabatic decay is comparatively fast [i.e., the cases marked in Fig. 2(a) with symbols]. Other sources of decay would have to be considered as well, including motional effects and collisions processes that arise from the monopole and dipole moments of the Rydberg ions. Future work on Rydberg-ion molecules may be devoted to studies of decay processes, investigation of the quantum interference effect highlighted in Fig. 3, and

studies of nonadiabatic decay on other potential-energy curves evident in Fig. 1(b) or in cesium. The formalism discussed here could also be applied to study nonadiabatic processes in other types of Rydberg molecules.

Note added. Recently, an observation of RAIMs has been reported [73] together with vibrational-ground-state lifetime measurements of $11.5 \pm 1.0\,\mu$s for $n = 54$ and $2.6 \pm 0.2\,\mu$s for $n = 69$, notably smaller than the lifetimes due to nonadiabatic effects predicted here. These experimental results are about one order of magnitude smaller than even the radiative lifetimes of the corresponding Rydberg states. The disagreement may be due to decay channels other than nonadiabatic decay, possibly triggered by stray electric fields or collisions with electrons or other particles. Future research will be required to shed light on the matter.

ACKNOWLEDGMENTS

We thank Bineet Kumar Dash and Ansh Shah for useful discussions. This work was supported by NSF Grant No. PHY-2110049 and in part through computational resources and services provided by Advanced Research Computing at the University of Michigan, Ann Arbor.

[1] J. P. Shaffer, S. T. Rittenhouse, and H. R. Sadeghpour, Ultracold Rydberg molecules, Nat. Commun. **9**, 1965 (2018).
[2] C. Fey, F. Hummel, and P. Schmelcher, Ultralong-range Rydberg molecules, Mol. Phys. **118**, e1679401 (2020).
[3] C. H. Greene, A. S. Dickinson, and H. R. Sadeghpour, Creation of Polar and Nonpolar Ultra-Long-Range Rydberg Molecules, Phys. Rev. Lett. **85**, 2458 (2000).
[4] V. Bendkowsky, B. Butscher, J. Nipper, J. P. Shaffer, R. Löw, and T. Pfau, Observation of ultralong-range Rydberg molecules, Nature (London) **458**, 1005 (2009).
[5] E. L. Hamilton, C. H. Greene, and H. R. Sadeghpour, Shape-resonance-induced long-range molecular Rydberg states, J. Phys. B **35**, L199 (2002).
[6] V. Bendkowsky, B. Butscher, J. Nipper, J. B. Balewski, J. P. Shaffer, R. Löw, T. Pfau, W. Li, J. Stanojevic, T. Pohl, and J. M. Rost, Rydberg Trimers and Excited Dimers Bound by Internal Quantum Reflection, Phys. Rev. Lett. **105**, 163201 (2010).
[7] J. Tallant, S. T. Rittenhouse, D. Booth, H. R. Sadeghpour, and J. P. Shaffer, Observation of Blueshifted Ultralong-Range Cs_2 Rydberg Molecules, Phys. Rev. Lett. **109**, 173202 (2012).
[8] M. A. Bellos, R. Carollo, J. Banerjee, E. E. Eyler, P. L. Gould, and W. C. Stwalley, Excitation of Weakly Bound Molecules to Trilobitelike Rydberg States, Phys. Rev. Lett. **111**, 053001 (2013).
[9] D. A. Anderson, S. A. Miller, and G. Raithel, Photoassociation of Long-Range *nD* Rydberg Molecules, Phys. Rev. Lett. **112**, 163201 (2014).
[10] B. J. DeSalvo, J. A. Aman, F. B. Dunning, T. C. Killian, H. R. Sadeghpour, S. Yoshida, and J. Burgdörfer, Ultra-long-range Rydberg molecules in a divalent atomic system, Phys. Rev. A **92**, 031403(R) (2015).
[11] M. Peper and J. Deiglmayr, Heteronuclear Long-Range Rydberg Molecules, Phys. Rev. Lett. **126**, 013001 (2021).
[12] D. A. Anderson, S. A. Miller, and G. Raithel, Angular-momentum couplings in long-range Rb_2 Rydberg molecules, Phys. Rev. A **90**, 062518 (2014).
[13] K. S. Kleinbach, F. Meinert, F. Engel, W. J. Kwon, R. Löw, T. Pfau, and G. Raithel, Photoassociation of Trilobite Rydberg Molecules via Resonant Spin-Orbit Coupling, Phys. Rev. Lett. **118**, 223001 (2017).
[14] M. T. Eiles and C. H. Greene, Hamiltonian for the inclusion of spin effects in long-range Rydberg molecules, Phys. Rev. A **95**, 042515 (2017).
[15] M. Deiß, S. Haze, J. Wolf, L. Wang, F. Meinert, C. Fey, F. Hummel, P. Schmelcher, and J. Hecker Denschlag, Observation of spin-orbit-dependent electron scattering using long-range Rydberg molecules, Phys. Rev. Research **2**, 013047 (2020).
[16] H. Saßmannshausen, F. Merkt, and J. Deiglmayr, Experimental Characterization of Singlet Scattering Channels in Long-Range Rydberg Molecules, Phys. Rev. Lett. **114**, 133201 (2015).
[17] F. Böttcher, A. Gaj, K. M. Westphal, M. Schlagmüller, K. S. Kleinbach, R. Löw, T. C. Liebisch, T. Pfau, and S. Hofferberth, Observation of mixed singlet-triplet Rb_2 Rydberg molecules, Phys. Rev. A **93**, 032512 (2016).
[18] F. Engel, T. Dieterle, F. Hummel, C. Fey, P. Schmelcher, R. Löw, T. Pfau, and F. Meinert, Precision Spectroscopy of Negative-Ion Resonances in Ultralong-Range Rydberg Molecules, Phys. Rev. Lett. **123**, 073003 (2019).
[19] J. L. MacLennan, Y.-J. Chen, and G. Raithel, Deeply bound $(24D_J + 5S_{1/2})$ ^{87}Rb and ^{85}Rb molecules for eight spin couplings, Phys. Rev. A **99**, 033407 (2019).
[20] B. Butscher, J. Nipper, J. B. Balewski, L. Kukota, V. Bendkowsky, R. Löw, and T. Pfau, Atom-molecule coherence for ultralong-range Rydberg dimers, Nat. Phys. **6**, 97 (2010).
[21] B. Butscher, V. Bendkowsky, J. Nipper, J. B. Balewski, L. Kukota, R Löw, T. Pfau, W. Li, T. Pohl, and J. M. Rost, Lifetimes of ultralong-range Rydberg molecules in vibrational ground and excited states, J. Phys. B **44**, 184004 (2011).
[22] F. Camargo, J. D. Whalen, R. Ding, H. R. Sadeghpour, S. Yoshida, J. Burgdörfer, F. B. Dunning, and T. C. Killian, Lifetimes of ultra-long-range strontium Rydberg molecules, Phys. Rev. A **93**, 022702 (2016).
[23] A. A. Khuskivadze, M. I. Chibisov, and I. I. Fabrikant, Adiabatic energy levels and electric dipole moments of Rydberg states of Rb_2 and Cs_2 dimers, Phys. Rev. A **66**, 042709 (2002).
[24] W. Li, T. Pohl, J. M. Rost, Seth T. Rittenhouse, H. R. Sadeghpour, J. Nipper, B. Butscher, J. B. Balewski, V. Bendkowsky, R. Löw, and T. Pfau, A homonuclear molecule with a permanent electric dipole moment, Science **334**, 1110 (2011).
[25] S. Bai, X. Han, J. Bai, Y. Jiao, J. Zhao, S. Jia, and G. Raithel, Cesium $nD_J + 6S_{1/2}$ Rydberg molecules and their permanent electric dipole moments, Phys. Rev. Research **2**, 033525 (2020).
[26] D. Booth, S. T. Rittenhouse, J. Yang, H. R. Sadeghpour, and J. P. Shaffer, Production of trilobite Rydberg molecule dimers with kilo-Debye permanent electric dipole moments, Science **348**, 99 (2015).
[27] T. Niederprüm, O. Thomas, T. Eichert, C. Lippe, J. Pérez-Ríos, C. H. Greene, and H. Ott, Observation of pendular butterfly Rydberg molecules, Nat. Commun. **7**, 12820 (2016).

[28] I. Lesanovsky, P. Schmelcher, and H. R. Sadeghpour, Ultralong-range Rydberg molecules exposed to a magnetic field, J. Phys. B **39**, L69 (2006).

[29] F. Hummel, C. Fey, and P. Schmelcher, Alignment of *s*-state Rydberg molecules in magnetic fields, Phys. Rev. A **99**, 023401 (2019).

[30] F. Hummel, K. Keiler, and P. Schmelcher, Electric-field-induced wave-packet dynamics and geometrical rearrangement of trilobite Rydberg molecules, Phys. Rev. A **103**, 022827 (2021).

[31] C. Boisseau, I. Simbotin, and R. Côté, Macrodimers: Ultralong Range Rydberg Molecules, Phys. Rev. Lett. **88**, 133004 (2002).

[32] K. R. Overstreet, A. Schwettmann, J. Tallant, D. Booth, and J. P. Shaffer, Observation of electric-field-induced Cs Rydberg atom macrodimers, Nat. Phys. **5**, 581 (2009).

[33] H. Saßmannshausen and J. Deiglmayr, Observation of Rydberg-Atom Macrodimers: Micrometer-Sized Diatomic Molecules, Phys. Rev. Lett. **117**, 083401 (2016).

[34] N. Samboy and R. Côté, Rubidium Rydberg linear macrotrimers, Phys. Rev. A **87**, 032512 (2013).

[35] R. J. Le Roy, Long-range potential coefficients from RKR turning points: C_6 and C_8 for $B(3\Pi^+_{Ou})$-state Cl_2, Br_2, and I_2, Can. J. Phys. **52**, 246 (1974).

[36] K. Singer, J. Stanojevic, M. Weidemüller, and R. Côté, Long-range interactions between alkali Rydberg atom pairs correlated to the ns-ns, np-np and nd-nd asymptotes, J. Phys. B **38**, S295 (2005).

[37] A. Schwettmann, J. Crawford, K. R. Overstreet, and J. P. Shaffer, Cold Cs Rydberg-gas interactions, Phys. Rev. A **74**, 020701(R) (2006).

[38] J. Deiglmayr, H. Saßmannshausen, P. Pillet, and F. Merkt, Observation of Dipole-Quadrupole Interaction in an Ultracold Gas of Rydberg Atoms, Phys. Rev. Lett. **113**, 193001 (2014).

[39] L. G. Marcassa and J. P. Shaffer, Interactions in ultracold Rydberg gases, Adv. At. Mol. Opt. Phys. **63**, 47 (2014).

[40] N. Samboy, J. Stanojevic, and R. Côté, Formation and properties of Rydberg macrodimers, Phys. Rev. A **83**, 050501(R) (2011).

[41] M. Kiffner, H. Park, W. Li, and T. F. Gallagher, Dipole-dipole-coupled double-Rydberg molecules, Phys. Rev. A **86**, 031401(R) (2012).

[42] X. Han, S. Bai, Y. Jiao, L. Hao, Y. Xue, J. Zhao, S. Jia, and G. Raithel, Cs $62D_J$ Rydberg-atom macrodimers formed by long-range multipole interaction, Phys. Rev. A **97**, 031403(R) (2018).

[43] X. Han, S. Bai, Y. Jiao, G. Raithel, J. Zhao, and S. Jia, Adiabatic potentials of cesium nD_2 Rydberg-Rydberg macrodimers, J. Phys. B **52**, 135102 (2019).

[44] S. Hollerith, J. Zeiher, J. Rui, A. Rubio-Abadal, V. Walther, T. Pohl, D. M. Stamper-Kurn, I. Bloch, and C. Gross, Quantum gas microscopy of Rydberg macrodimers, Science **364**, 664 (2019).

[45] A. Schwettmann, K. R. Overstreet, J. Tallant, and J. P. Shaffer, Analysis of long-range Cs Rydberg potential wells, J. Mod. Opt. **54**, 2551 (2007).

[46] S. Hollerith, J. Rui, A. Rubio-Abadal, K. Srakaew, D. Wei, J. Zeiher, C. Gross, and I. Bloch, Microscopic electronic structure tomography of Rydberg macrodimers, Phys. Rev. Research **3**, 013252 (2021).

[47] A. Duspayev, X. Han, M. A. Viray, L. Ma, J. Zhao, and G. Raithel, Long-range Rydberg-atom–ion molecules of Rb and Cs, Phys. Rev. Research **3**, 023114 (2021).

[48] M. Deiß, S. Haze, and J. Hecker Denschlag, Long-range atom-ion Rydberg molecule: A novel molecular binding mechanism, Atoms **9**, 34 (2021).

[49] S. Schmid, A. Härter, and J. H. Denschlag, Dynamics of a Cold Trapped Ion in a Bose-Einstein Condensate, Phys. Rev. Lett. **105**, 133202 (2010).

[50] T. Secker, R. Gerritsma, A. W. Glaetzle, and A. Negretti, Controlled long-range interactions between Rydberg atoms and ions, Phys. Rev. A **94**, 013420 (2016).

[51] T. Secker, N. Ewald, J. Joger, H. Fürst, T. Feldker, and R. Gerritsma, Trapped Ions in Rydberg-Dressed Atomic Gases, Phys. Rev. Lett. **118**, 263201 (2017).

[52] T. Schmid, C. Veit, N. Zuber, R. Löw, T. Pfau, M. Tarana, and M. Tomza, Rydberg Molecules for Ion-Atom Scattering in the Ultracold Regime, Phys. Rev. Lett. **120**, 153401 (2018).

[53] N. V. Ewald, T. Feldker, H. Hirzler, H. A. Fürst, and R. Gerritsma, Observation of Interactions Between Trapped Ions and Ultracold Rydberg Atoms, Phys. Rev. Lett. **122**, 253401 (2019).

[54] L. Wang, M. Deiß, G. Raithel, and J. H. Denschlag, Optical control of atom-ion collisions using a Rydberg state, J. Phys. B **53**, 134005 (2020).

[55] H. Hirzler and J. Pérez-Ríos, Rydberg atom-ion collisions in cold environments, Phys. Rev. A **103**, 043323 (2021).

[56] T. Dieterle, M. Berngruber, C. Hölzl, R. Löw, K. Jachymski, T. Pfau, and F. Meinert, Transport of a Single Cold Ion Immersed in a Bose-Einstein Condensate, Phys. Rev. Lett. **126**, 033401 (2021).

[57] M. Born and K. Huang, *Dynamical Theory of Crystal Lattices* (Oxford University, New York, 1954).

[58] F. Agostini and B. F. E. Curchod, Different flavors of nonadiabatic molecular dynamics, WIREs Comput. Mol. Sci. **9**, e1417 (2019).

[59] M. Schlagmüller, T. C. Liebisch, F. Engel, K. S. Kleinbach, F. Böttcher, U. Hermann, K. M. Westphal, A. Gaj, R. Löw, S. Hofferberth, T. Pfau, J. Pérez-Ríos, and C. H. Greene, Ultracold Chemical Reactions of a Single Rydberg Atom in a Dense Gas, Phys. Rev. X **6**, 031020 (2016).

[60] F. Hummel, M. T. Eiles, and P. Schmelcher, Synthetic Dimension-Induced Conical Intersections in Rydberg Molecules, Phys. Rev. Lett. **127**, 023003 (2021).

[61] M. Born and R. Oppenheimer, Zur Quantentheorie der Molekeln, Ann. Phys. (Leipzig) **389**, 457 (1927).

[62] .S. E. Koonin and D. C. Meredith, *Computational Physics Fortran Version* (Addison-Wesley, Reading, MA, 1990), pp. 169–180.

[63] J. G. Muga, J. P. Palao, B. Navarro, and I. L. Egusquiza, Complex absorbing potentials, Phys. Rep. **395**, 357 (2004).

[64] T. F. Gallagher, *Rydberg Atoms* (Cambridge University, Cambridge, England, 2005), Vol. 3.

[65] M. Traxler, R. E. Sapiro, K. Lundquist, E. P. Power, and G. Raithel, Coupled internal-state and center-of-mass dynamics of Rydberg atoms in a magnetic guide, Phys. Rev. A **87**, 053418 (2013).

[66] D. A. Anderson, A. Schwarzkopf, R. E. Sapiro, and G. Raithel, Production and trapping of cold circular Rydberg atoms, Phys. Rev. A **88**, 031401(R) (2013).

[67] D. B. Branden, T. Juhasz, T. Mahlokozera, C. Vesa, R. O. Wilson, M. Zheng, A. Kortyna, and D. A. Tate, Radiative lifetime measurements of rubidium Rydberg states, J. Phys. B **43**, 015002 (2009).

[68] I. I. Beterov, I. I. Ryabtsev, D. B. Tretyakov, and V. M. Entin, Quasiclassical calculations of blackbody-radiation-induced depopulation rates and effective lifetimes of Rydberg *ns*, *np*, and *nd* alkali-metal atoms with $n \leqslant 80$, Phys. Rev. A **79**, 052504 (2009).

[69] N. V. Vitanov, Transition times in the Landau-Zener model, Phys. Rev. A **59**, 988 (1999).

[70] S. N. Shevchenko, S. Ashhab, and F. Nori, Landau-Zener-Stückelberg interferometry, Phys. Rep. **492**, 1 (2010).

[71] N. Balakrishnan, B. D. Esry, H. R. Sadeghpour, S. T. Cornett, and M. J. Cavagnero, Quantum wave-packet dynamics of the photodissociation of LiF, Phys. Rev. A **60**, 1407 (1999).

[72] S. T. Cornett, H. R. Sadeghpour, and M. J. Cavagnero, Interferometric Line Shape Modulation in Alkali-Halide Photoabsorption, Phys. Rev. Lett. **82**, 2488 (1999).

[73] N. Zuber, V. S. V. Anasuri, M. Berngruber, Y.-Q. Zou, F. Meinert, R. Löw, and T. Pfau, Spatial imaging of a novel type of molecular ions, arXiv:2111.02680 (2021).